



Short communication

# A method for preserving nominally-resolved flow patterns in low-resolution ocean simulations: Dynamical system reconstruction

I. Shevchenko<sup>a,\*</sup>, P. Berloff<sup>a,b</sup>

<sup>a</sup>*Department of Mathematics, Imperial College London, Huxley Building, 180 Queen's Gate, London, SW7 2AZ, UK*

<sup>b</sup>*Institute of Numerical Mathematics of the Russian Academy of Sciences, Moscow, Russia*

---

## Abstract

1 Accurate representation of large-scale flow patterns in low-resolution ocean simulations is one of the most challenging  
2 problems in ocean modelling. The main difficulty is to correctly reproduce effects of unresolved small scales on the  
3 resolved large scales. For this purpose, most of current research is focused on development of parameterisations  
4 directly accounting for the small scales. In this work we propose an alternative to the mainstream ideas by showing  
5 how to reconstruct a dynamical system from the available reference solution data (our proxy for observations) and,  
6 then, how to use this system for modelling not only large-scale but also nominally-resolved flow patterns at low  
7 resolutions. This approach is advocated as a part of the novel framework for data-driven hyper-parameterisation of  
8 mesoscale oceanic eddies in non-eddy-resolving models. The main characteristic of this framework is that it does  
9 not require to know the physics behind large-small scale interactions to reproduce both large and small scales in  
10 low-resolution ocean simulations. We tested it in the context of a three-layer, statistically equilibrated, steadily  
11 forced quasigeostrophic model for the beta-plane configuration and showed that non-eddy-resolving solution can  
12 be substantially improved towards the reference eddy-resolving benchmark. The proposed methodology robustly  
13 allows to retrieve a system of equations governing reduced dynamics of the observed data, while the additional  
14 adaptive nudging counteracts numerical instabilities by keeping solutions in the region of phase space occupied  
15 by the reference fields. Remarkably, its solutions simulate not only large-scale but also small-scale flow features,  
16 which can be nominally resolved by the low-resolution grid. In addition, the proposed method reproduces realistic  
17 vortex trajectories. One of the important and general conclusions that can be drawn from our results is that not  
18 only mesoscale eddy parameterization is possible in principle but also it can be highly accurate (up to reproducing  
19 individual vortices) for significantly reduced dynamics (down to 30 degrees of freedom). This conclusion provides  
20 great optimism for the ongoing parameterization studies, which are still far away from being completed.

© 2011 Published by Elsevier Ltd.

*Keywords:* Ocean general circulation and dynamics, Multi-layer quasi-geostrophic model, Mesoscale eddies and parameterizations, Dynamical system reconstruction, Adaptive nudging

---

\*Corresponding author at:

*Email address:* [i.shevchenko@imperial.ac.uk](mailto:i.shevchenko@imperial.ac.uk) (I. Shevchenko)

## 21 1. Introduction

22 It is typical of low-resolution ocean simulations to have significantly distorted or even absent large-scale  
 23 flow structures that are otherwise present in the high-resolution simulations. This failure is due to missing  
 24 effects of the small scales, which are not adequately resolved in low-resolution simulations. To mitigate the  
 25 problem, many parameterisations for both comprehensive and idealized ocean models have been proposed  
 26 (e.g., [Gent and McWilliams \(1990\)](#); [Duan and Nadiga \(2007\)](#); [Frederiksen et al. \(2012\)](#); [Jansen and Held](#)  
 27 [\(2014\)](#); [Mana and Zanna \(2014\)](#); [Cooper and Zanna \(2015\)](#); [Grooms et al. \(2015\)](#); [Berloff \(2015, 2016,](#)  
 28 [2018\)](#); [Danilov et al. \(2019\)](#); [Ryzhov et al. \(2019\)](#); [Juricke et al. \(2020a,b\)](#); [Cotter et al. \(2019\)](#); [Ryzhov et al.](#)  
 29 [\(2020\)](#); [Cotter et al. \(2020a,b,c\)](#)), but overall the problem remains largely unresolved for several reasons.  
 30 First, defining the small and large scales is ambiguous, because they are not separated by a clear spectral  
 31 gap or otherwise. Second, definition of the small and large scales should be consistent with the specific  
 32 resolving capabilities of a low-resolution model in which their interactions are to be parameterized. Third,  
 33 dynamical interactions across the scales are remarkably complex, as well as spatially inhomogeneous and  
 34 non-stationary.

35 In this work we have further developed the hyper-parameterisation approach to reproduce the effects  
 36 of mesoscale oceanic eddies on the large-scale ocean circulation. The main characteristic of this approach  
 37 is that it does not require to know the physics behind large-small scale interactions to reproduce them.  
 38 Complimentary to the mainstream physics-based perspective, we propose to deal with the eddy effects from  
 39 the dynamical systems point of view, and interpret the lack of them as the persistent tendency of phase space  
 40 trajectories representing the low-resolution solution to escape the right region of the corresponding phase  
 41 space, which is occupied by the reference eddy-resolving solution. Therefore, we approach the problem from a  
 42 different direction: instead of parameterizing small-scale effects, we retrieve an underlying dynamical system  
 43 and use it to model evolution of the nominally-resolved flow patterns at low resolutions. The nominally-  
 44 resolved flow patterns are those that are resolved by the grid. In our case, we need at least 7 grid points per  
 45 the flow pattern to ensure it is resolved, since we use the CABARET scheme ([Karabasov et al., 2009](#)), while  
 46 conventional methods would require at least 10 points. For example, a vortex of 70km in diameter requires  
 47 the grid step to be at least 10km. Although the basic idea has long research history, our application of  
 48 it is novel, and the proposed methodology has many novel features. Let us first discuss below the relevant  
 49 background.

50 Retrieving reduced equations underlying the observed flow evolution is one of the most challenging  
 51 problems in dynamical systems (e.g.,([Aguirre and Letellier, 2009](#); [Brunton et al., 2016](#))). Although, this  
 52 field has been researched for decades, most of the efforts used low-dimensional dynamical systems with 3-5  
 53 degrees of freedom (e.g., [Brunton et al. \(2017\)](#); [Mangiarotti and Huc \(2019\)](#)), and even this turned out  
 54 difficult. The other problem is about frequent numerical instabilities of the retrieved dynamical systems  
 55 (e.g., [Sceller et al. \(1999\)](#)). This implies that applying known methodologies for thousands of degrees of  
 56 freedom, typical for describing low-resolution oceanic flows, is unfeasible.

57 For developing and testing the approach, we considered an intermediate-complexity, quasigeostrophic,  
 58 eddy-resolving model of the wind-driven midlatitude ocean circulation — this is a respected and widely used  
 59 (e.g., [Siegel et al. \(2001\)](#); [Karabasov et al. \(2009\)](#); [Shevchenko and Berloff \(2016\)](#); [Shevchenko et al. \(2016\)](#)  
 60 and references there in) paradigm for process studies involving large-/small-scale turbulent interactions and  
 61 their parameterizations. To mitigate the model size problem, we applied the Empirical Orthogonal Function  
 62 (EOF) analysis ([Preisendorfer, 1988](#); [Hannachi et al., 2007](#)) to the reference flow, defined here as the high-  
 63 resolution solution subsampled on a coarse grid, and reconstructed a dynamical system for the evolving  
 64 Principal Components (PCs) corresponding to the leading EOFs. Successful examples of reduced-order  
 65 modelling with EOF-PC description can be found in ([Kondrashov and Berloff, 2015](#); [Kondrashov et al.,](#)  
 66 [2018](#)). Other types of space reduction are possible and can improve the outcome even further, but they are  
 67 not considered in this study. To resolve the problem with numerical instabilities, we used adaptive nudging

68 methodology, which is an upgraded extension of the nudging method proposed in (Shevchenko and Berloff,  
69 2021).

## 70 2. The method

71 The main objective of this study is to reconstruct a dynamical system from the reference solution (say  
72  $\mathbf{x}(t)$ ,  $\mathbf{x} \in \mathbb{R}^n$ ); the reference solution is the high-resolution solution projected onto the coarser grid. Note that  
73  $\mathbf{x}(t)$  cannot be evolved in terms of  $\mathbf{x}(t)$  only (without knowledge of the high-resolution solution), i.e. the  
74 evolution equation for  $\mathbf{x}(t)$  is not closed. This is why we reconstruct a dynamical system for the evolution  
75 of  $\mathbf{x}(t)$ .

76 This dynamical system is meant to correctly simulate the reference large-scale flow patterns on a low-  
77 resolution grid. The full dimensionality of the problem is the total number of the grid nodes, and for the  
78 reconstructed dynamical system we aim to reduce it by orders of magnitude via EOFs/PCs decomposition  
79 of the reference data. Next, we formulate general dynamical system in terms of the leading PCs:

$$\mathbf{y}'(t) = \mathbf{F}(\mathbf{y}), \quad \mathbf{y} \in \mathbb{R}^m, \quad t \in [0, \tilde{T}], \quad m \ll n, \quad (1)$$

80 where the PCs are combined in the vector and denoted by  $\mathbf{y}(t)$ , and the dash means time differentiation.  
81 In our case the dimensionality has been eventually reduced by three orders of magnitude (from  $n = 16441$   
82 to  $m = 30$ ).

83 In (1) we used 30 leading PCs that captured 98% of the reference flow variance. The right hand side  
84 of (1) is approximated with polynomial of order two in all the variables,  $\mathbf{P}(\mathbf{y})$ , and with the Fourier series,  
85  $\mathcal{F}(\mathbf{y})$ , containing 50 leading harmonics:

$$\mathbf{F}(\mathbf{y}) \approx \mathbf{P}(\mathbf{y}) + \mathcal{F}(\mathbf{y}), \quad (2)$$

86 where

$$\mathbf{P}(\mathbf{y}) := a_0 + \sum_{i=1}^{30} a_i y_i + b_i y_i^2 + c_i y_i y_j, \quad j = 1, \dots, m, \quad i \neq j, \quad (3)$$

87 and

$$\mathcal{F}(\mathbf{y}) := \sum_{k=1}^{25} d_k \cos\left(\frac{2\pi k t}{\tilde{T}}\right) + e_k \sin\left(\frac{2\pi k t}{\tilde{T}}\right), \quad (4)$$

88 with unknown coefficients  $\mathbf{c} = \{a_0, a_i, b_i, c_i, d_k, e_k\}$ ,  $i = 1, \dots, 30$ ,  $k = 1, \dots, 25$  to be defined with the least  
89 squares method from the system of equations:

$$\mathbf{A}\mathbf{c} = \mathbf{y}'. \quad (5)$$

90 The derivative on the right hand side of (5) is approximated with the forward finite difference, and it is  
91 computed over the time interval  $[0, \tilde{T}]$  for which the leading PCs (computed from the reference solution)  
92 are available.

93 Note that  $\mathbf{F}(\mathbf{y})$  can be approximated differently, and its optimal choice (beyond the scope of this work)  
94 is a challenge for the dynamical system reconstruction. Without proper information for tailoring the right  
95 hand side more specifically, a polynomial expansion is justified by the Weierstrass approximation theorem,  
96 while the use of the Fourier series allows one to approximate the mean flow more accurately. We will get  
97 back to this choice when discussing the results. We note that the choice of the polynomial basis is justified by  
98 the Weierstrass theorem as one can approximate the right hand side with a desired order of accuracy using  
99 polynomial functions. It does not mean though that the Weierstrass theorem justifies the use of quadratic  
100 polynomials for the dynamical system reconstruction as the latter is not guaranteed to be accurate even if  
101 the right hand side is accurately approximated.

102 Having approximated  $\mathbf{F}(\mathbf{y})$  up to a given order of accuracy, one can solve the reconstructed dynamical  
 103 system

$$\mathbf{z}'(t) = \mathbf{P}(\mathbf{z}) + \mathcal{F}(\mathbf{z}), \quad \mathbf{z} \in \mathbb{R}^m, \quad t \in [0, T], \quad T > \tilde{T}. \quad (6)$$

104 Note that this system is integrated over a time interval which is longer (here, 2 times longer) than that  
 105 of the original system (1). In all further simulations we will have  $\tilde{T} = 2$  years and  $T = 4$  years. However,  
 106 an accurate approximation of  $\mathbf{F}(\mathbf{y})$  does not guarantee that system (6) can be easily solved, because the  
 107 integration errors can quickly contaminate the solution and result in severe numerical instability — this is  
 108 what actually happened in our case. In order to stabilize the numerical integration, we used the nudging  
 109 methodology (Shevchenko and Berloff, 2021):

$$\mathbf{z}'(t) = \mathbf{P}(\mathbf{z}) + \mathcal{F}(\mathbf{z}) + \eta \left( \frac{1}{N} \sum_{k \in \mathcal{U}(\mathbf{z}(t))} \mathbf{y}(t_k) - \mathbf{z}(t) \right), \quad t \in [0, T], \quad (7)$$

110 where  $\mathcal{U}(\mathbf{z}(t))$  is a neighbourhood of  $\mathbf{z}(t)$ , and index  $k$  is the timestep of the corresponding PC  $\mathbf{y}(t_k)$ ; the  
 111 timestep of the PC is the timestep with which the actual data for the EOF analysis was generated. The  
 112 notation  $k \in \mathcal{U}(\mathbf{z}(t))$  means that  $k$ 's are taken for those  $\mathbf{y}(t_k)$  that are in the neighbourhood of  $\mathbf{z}(t)$ . The  
 113 neighbourhood is computed in  $l_2$  norm as the average of  $N = 5$  points nearest to the solution  $\mathbf{z}(t)$ . Note  
 114 that the number of neighbourhood points is a parameter, and its sensitivity should be explored and taken  
 115 into account for each application of the proposed methodology. We have defined its value from a series of  
 116 experiments with values 2, 5, 10, 20;  $N = 5$  gives the most accurate solution.

117 Having solved equation (7), we approximated the reference solution by using the leading EOF-PC pairs  
 118 as follows:

$$\mathbf{x}(t) \approx \sum_{i=1}^m z_i(t) \mathbf{E}_i, \quad (8)$$

119 with  $\mathbf{E}_i$  and  $z_i$  being the  $i$ -th EOF and PC, respectively. The choice of  $m$  results from the variability of the  
 120 reference solution to be reproduced.

121 Note that  $N$  in equation (7) can be made time-dependent and adaptive, like the nudging coefficient  $\eta$ ,  
 122 which is the other important parameter. In order to make the numerical integration stable with the Euler  
 123 method, we used the following adaptive nudging:

$$\eta(t_i) = \begin{cases} \eta(t_{i-1}) + \eta_h & \text{if } \sigma(\mathbf{z}(t_i)) > \max_{t \in [0, \tilde{T}]} \sigma(\mathbf{y}(t)), \\ \eta(t_{i-1}) - \eta_h & \text{if } \sigma(\mathbf{z}(t_i)) \leq \max_{t \in [0, \tilde{T}]} \sigma(\mathbf{y}(t)), \\ 0 & \text{if } \eta(t_{i-1}) - \eta_h < 0. \end{cases} \quad i = 1, 2, \dots \quad (9)$$

124 with  $\sigma$  being the standard deviation,  $\eta_h = 0.001$ , and  $\eta(t_0) = 0$ .

125 We opted for an adaptive nudging, as it keeps the system within a neighbourhood of the phase space  
 126 region occupied by the reference solution. As an alternative, a constant  $\eta$  can be also used with some tuning  
 127 and caution, keeping in mind that its small value may not be enough for keeping the solution within the  
 128 right region and its large value may result in an over-stabilized solution with suppressed flow variability  
 129 (slow flow dynamics).

### 130 3. Multilayer quasi-geostrophic model

131 We consider a 3-layer quasi-geostrophic (QG) model with forcing and dissipation for the evolution of the  
 132 potential vorticity (PV) anomaly  $\mathbf{q} = (q_1, q_2, q_3)$  in domain  $\Omega$  (Pedlosky, 1987):

$$\partial_t q_j + \mathbf{J}(\psi_j, q_j + \beta y) = \delta_{1j} F_w - \delta_{j3} \mu \nabla^2 \psi_j + \nu \nabla^4 \psi_j, \quad j = 1, 2, 3, \quad (10)$$

133 where  $J(f, g) = f_x g_y - f_y g_x$ ,  $\delta_{ij}$  is the Kronecker symbol, and  $\boldsymbol{\psi} = (\psi_1, \psi_2, \psi_3)$  is the velocity streamfunction  
 134 in three layers. The planetary vorticity gradient is  $\beta = 2 \times 10^{-11} \text{ m}^{-1} \text{ s}^{-1}$ , the bottom friction parameter is  
 135  $\mu = 4 \times 10^{-8} \text{ s}^{-1}$ , and the lateral eddy viscosity is  $\nu = 50 \text{ m}^2 \text{ s}^{-1}$ . The asymmetric wind curl forcing, driving  
 136 the double-gyre ocean circulation, is given by

$$F_w = \begin{cases} -1.80 \pi \tau_0 \sin(\pi y / y_0), & y \in [0, y_0], \\ 2.22 \pi \tau_0 \sin(\pi(y - y_0) / (L - y_0)), & y \in [y_0, L], \end{cases}$$

137 with the wind stress amplitude  $\tau_0 = 0.03 \text{ N m}^{-2}$  and the tilted zero forcing line  $y_0 = 0.4L + 0.2x$ ,  $x \in [0, L]$ .  
 138 The computational domain  $\Omega = [0, L] \times [0, L] \times [0, H]$  is a closed, flat-bottom basin with  $L = 3840 \text{ km}$ , and  
 139 the total depth  $H = H_1 + H_2 + H_3$  given by the isopycnal fluid layers of depths (top to bottom):  $H_1 = 0.25 \text{ km}$ ,  
 140  $H_2 = 0.75 \text{ km}$ ,  $H_3 = 3.0 \text{ km}$ .

141 The PV anomaly  $\mathbf{q}$  and the velocity streamfunction  $\boldsymbol{\psi}$  are coupled through the system of elliptic equa-  
 142 tions:

$$\mathbf{q} = \nabla^2 \boldsymbol{\psi} - \mathbf{S} \boldsymbol{\psi}, \quad (11)$$

143 with the stratification matrix

$$\mathbf{S} = \begin{pmatrix} 1.19 \cdot 10^{-3} & -1.19 \cdot 10^{-3} & 0.0 \\ -3.95 \cdot 10^{-4} & 1.14 \cdot 10^{-3} & -7.47 \cdot 10^{-4} \\ 0.0 & -1.87 \cdot 10^{-4} & 1.87 \cdot 10^{-4} \end{pmatrix}.$$

144 The stratification parameters are given in units of  $\text{km}^{-2}$  and chosen so, that the first and second Rossby  
 145 deformation radii are  $Rd_1 = 40 \text{ km}$  and  $Rd_2 = 23 \text{ km}$ , respectively; the choice of these parameters is typical  
 146 for the North Atlantic, as it allows to simulate a more realistic than in different QG setups but yet idealized  
 147 eastward jet extension of the western boundary currents

148 System (10)-(11) is augmented with the integral mass conservation constraint (McWilliams, 1977):

$$\partial_t \iint_{\Omega} (\psi_j - \psi_{j+1}) \, dy dx = 0, \quad j = 1, 2 \quad (12)$$

149 with the zero initial condition, and with the partial-slip lateral boundary condition (Haidvogel et al., 1992):

$$(\partial_{\mathbf{nn}} \boldsymbol{\psi} - \alpha^{-1} \partial_{\mathbf{n}} \boldsymbol{\psi}) \Big|_{\partial \Omega} = 0, \quad (13)$$

151 where  $\alpha = 120 \text{ km}$  is the partial-slip parameter, and  $\mathbf{n}$  is the normal-to-wall unit vector; no-flow-through  
 152 boundary condition is also implemented (as part of the elliptic solver). The value of the parameter  $\alpha$  is  
 153 chosen based on the study by Shevchenko and Berloff (2015), where it has been shown that smaller values of  
 154  $\alpha$  inhibit the eastward jet extension penetration length and volume transport, while larger values have much  
 155 less pronounced influence on the jet. As with other governing parameters used in this study, our choice of  
 156  $\alpha$  is justified by a more realistic eastward jet. The QG system (10)-(13) is solved using the high-resolution  
 157 CABARET method, which is based on a second-order, non-dissipative and low-dispersive, conservative  
 158 advection scheme.

159 For this study we need both high- and low-resolution solutions. In order to compute them, we first spin  
 160 up the model (10)-(13) for 100 years and then solve it for the other 4 years on 2 uniform horizontal grids:  
 161  $513 \times 513$  (high resolution) and  $129 \times 129$  (low resolution). Note that all the parameters in the QG model are  
 162 held fixed for both high- and low-resolution setups. In order to obtain the reference solution (denoted as  $q_1$ ),  
 163 we project the high-resolution solution on the coarse grid  $129 \times 129$  by using point-to-point projection, i.e.  
 164 the high-resolution solution is subsampled at the low-resolution grid points, (Figure 1a). The low-resolution  
 165 solution (denoted as  $\widehat{q}_1$ ) is the solution of the QG model on grid  $129 \times 129$  (Figure 1b). Our goal is to find  
 166 a dynamical system that can model the leading PCs (which are then used to approximate the reference

167 solution given by (8)), so that the approximate solution (denoted as  $\tilde{q}_1$ ) simulates the reference large-scale  
 168 flow patterns in qualitatively correct way. We would like to draw the reader’s attention to the fact that in  
 169 the general description of the method the reference solution is denoted as  $\mathbf{x}(t)$ , while in the context of the  
 170 QG model  $\mathbf{x}(t) := q_1$ .

171 For the purpose of this work, it is enough to consider only the first layer, as it consists of both large-  
 172 and small-scale features (Figure 1a) which we aim to reproduce. Moreover, the upper layer is more difficult  
 173 to model than the deep ones. As seen in Figure 1a, the solution is characterized by the well-pronounced  
 174 eastward jet extension of the western boundary currents and surrounding small-scale coherent vortices. Both  
 175 of these features are missed in the low-resolution solution (Figure 1b) due to the under-resolved eddy effects.  
 176 In order to restore nominally-resolved flow patterns (the eastward jet and surrounding vortices), we first  
 177 reconstruct a reduced dynamical system (for the leading PCs) which is based on the second-order polynomials  
 178 and then the one based on the second-order polynomials and Fourier series. The solution corresponding to  
 179 the former is presented in Figure 1c. Although the snapshots show that both the eastward jet and vortices  
 180 are successfully reproduced, the time-mean flow significantly differs from the reference solution: the eastward  
 181 jet separation point is shifted north and the jet itself manifests fluctuations unseen in the reference solution.

182 For a better approximation we combined the second-order polynomial basis with the Fourier series. The  
 183 corresponding solution (8) computed from the leading EOF-PC pairs is significantly improved (Figure 1d),  
 184 mostly due to the better approximation of the PCs (Figure 2). The low-resolution solutions  $q_1^*$  and  $\tilde{q}_1$   
 185 (Figures 1c,d) have excessive spatial variance in the 4-year averages compared to the reference solution  $q_1$   
 186 (Figure 1a). This is improved by adding the Fourier basis (Figure 1d). Also, the low resolution solutions  
 187 have excessive time variance (Figure 1, standard deviation panels). This is made worse by adding the Fourier  
 188 basis (for example in the jet detachment region).

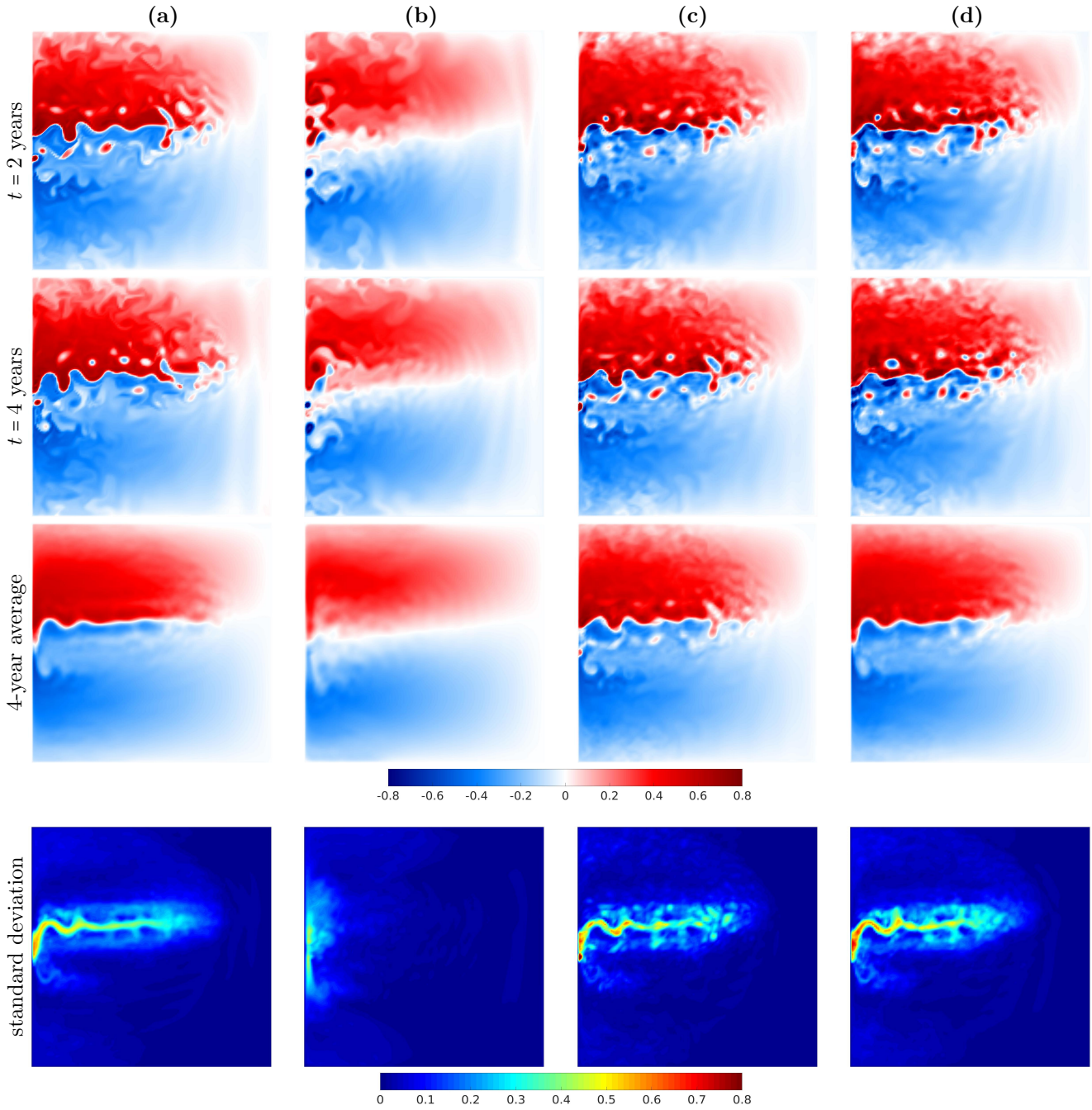


Figure 1: Shown is a series of snapshots, 4-year average, and standard deviation of the top layer PV anomaly of (a) the reference solution  $q_1$  (computed on grid  $513 \times 513$  and projected on grid  $129 \times 129$ ), (b) low-resolution solution  $\hat{q}_1$  computed on grid  $129 \times 129$ , (c) low-resolution solution  $q_1^*$  on grid  $129 \times 129$  (with the second-order polynomial basis used for the reconstruction), (d) low-resolution solution  $\hat{q}_1$  on grid  $129 \times 129$  (with the second-order polynomials and Fourier basis used for the reconstruction). The solution is given in units of  $[s^{-1} f_0^{-1}]$ , where  $f_0 = 0.83 \times 10^{-4} s^{-1}$  is the Coriolis parameter. The results in panels (c), (d) demonstrate that the proposed method preserves not only large-, but also small-scale features (nominally resolved on the coarse-grid) like those seen in the reference solution (a) but absent in the low-resolution solution (b).

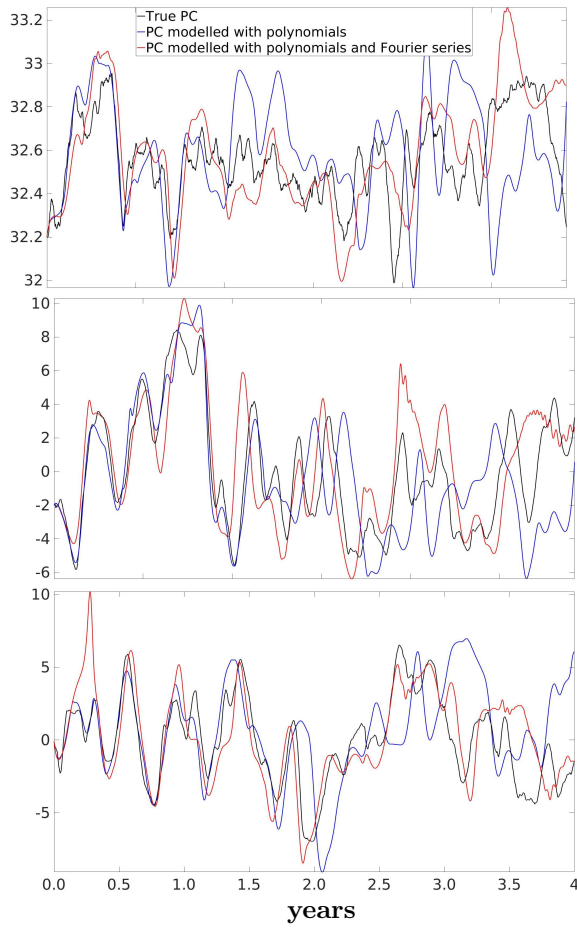


Figure 2: Shown are the first three leading PCs and their dependence on the basis functions used for the reconstruction of the dynamical system: true PC (black), PC modelled with the second-order polynomial-only basis (blue), and PC modelled with both the second-order polynomials and Fourier series (red). The results demonstrate that using the basis consisting of both the second-order polynomials and Fourier series yields significantly more accurate approximation of the PCs.



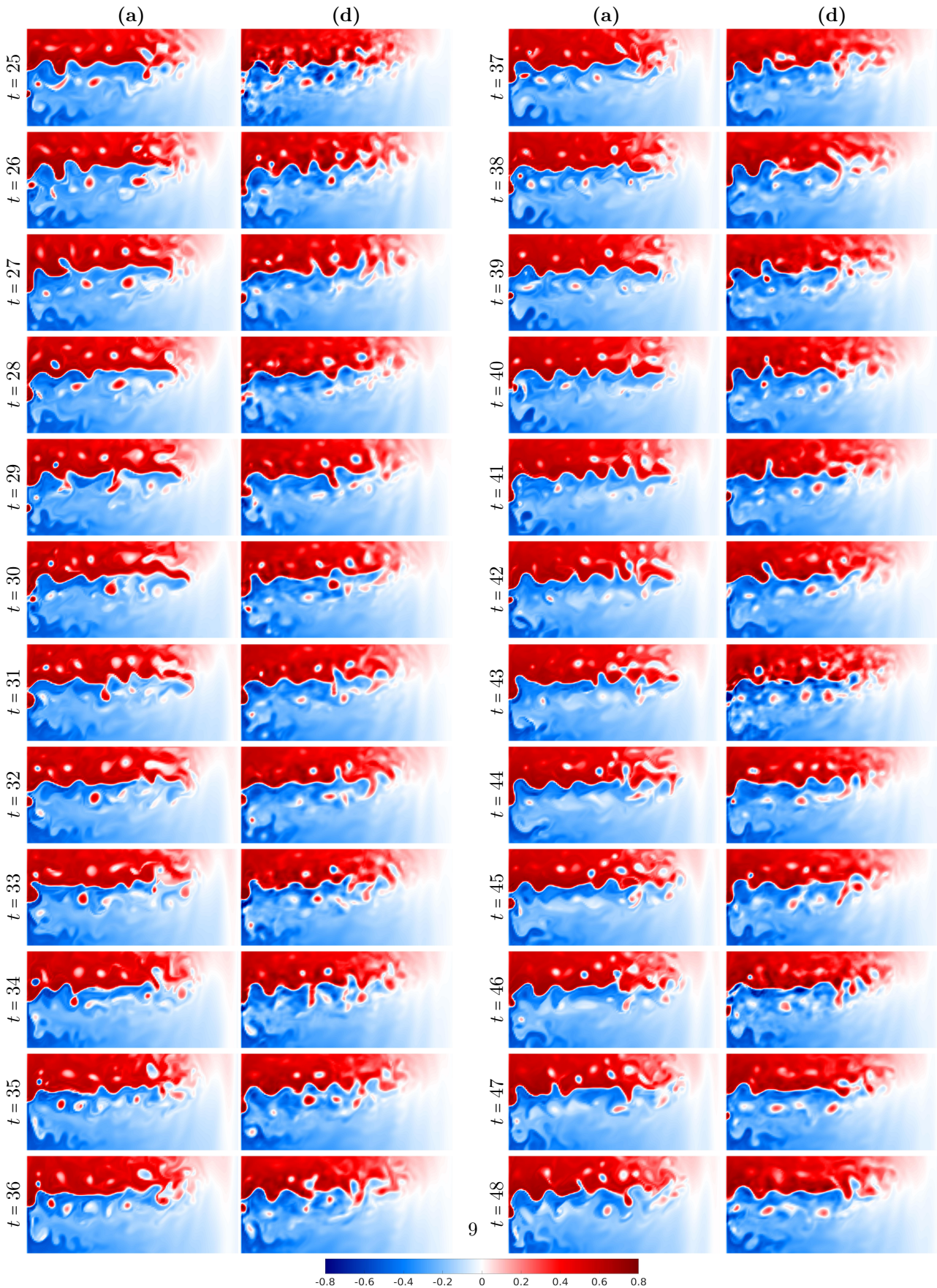


Figure 3: The same panels as in Figure 1 but with the time step 1 month. Shown is a neighbourhood of the eastward jet for the last two years of the 4-year long simulation. The results clearly demonstrate that not only the nominally-resolved flow structures (the eastward jet and coherent vortices) are present in the modelled solution but also realistic vortex trajectories are correctly reproduced.

189 Recall that the solution in Figure 1 is over 4 years, and only the first 2 years were used to reconstruct the  
 190 dynamical system. This shows that the proposed method preserves not only the large-scale flow structure but  
 191 also the small-scale flow features, all of them over a long time interval. It means that the proposed method  
 192 maintains the large-scale flow structure (the eastward jet extension of the western boundary currents) and  
 193 small-scale features (nominally resolved on the coarse grid eddies) akin to those of the reference solution.  
 194 Figure 3 shows that not only the nominally-resolved flow structures are present in the modelled solution but  
 195 also realistic vortex trajectories (vortices drift westward) are correctly reproduced. Moreover, vortices are  
 196 formed at the tip of the jet and through meanders along the jet. However, it does not mean that the exact  
 197 same individual eddies (vortices) in the sub-sampled high resolution solution are preserved. For example,  
 198 the individual eddies in Figures 1a,d and Figures 3a,d are different. Besides, the dispersion characteristics  
 199 of the reference and the reconstructed flow have not been checked and may be different. The ability of the  
 200 method to reproduce small-scale features may look surprising, but since these features were present in the  
 201 reference data, their reconstruction is a matter of the high-quality reconstruction of the dynamical system.

202 A key ingredient that makes the method work is the adaptive nudging which keeps the solution in the  
 203 right region of the phase space that is occupied by the reference solution. As an approximation of the  
 204 reference region, we used a sphere,  $S(\mathbf{q}_1)$ , centered at the time-mean of the solution,  $\langle \mathbf{q}_1 \rangle$ , and the sphere  
 205 radius,  $r$ , is the mean distance of the solution from the centre:

$$S(\mathbf{q}_1) := (\mathbf{q}_1 - \langle \mathbf{q}_1 \rangle)^2 - r^2 \leq 0, \quad \langle \mathbf{q}_1 \rangle := \frac{1}{T} \int_0^T \mathbf{q}_1(t) dt, \quad r := \frac{1}{T} \int_0^T \|\mathbf{q}_1(t) - \langle \mathbf{q}_1 \rangle\|_2 dt. \quad (14)$$

206 The mean distance between two points  $\mathbf{x}_1(t)$  and  $\mathbf{x}_2(t)$  in the phase space of the QG model is given by

$$\langle \mathcal{D}(\mathbf{x}_1, \mathbf{x}_2) \rangle := \frac{1}{T} \int_0^T \|\mathbf{x}_1(t) - \mathbf{x}_2(t)\|_2 dt. \quad (15)$$

207 The mean distance computed below is given in non-dimensional units.

208 The mean distances for the reference and low-resolution solutions are  $\langle \mathcal{D}(q_1, \bar{q}_1) \rangle = 11.9$  and  $\langle \mathcal{D}(\hat{q}_1, \bar{\hat{q}}_1) \rangle =$   
 209  $7.2$ , respectively, showing that the latter is confined in a smaller region. The  $l_2$ -norm distance between the  
 210 time means of these solutions (denoted as barred quantities) is  $\mathcal{D}(\bar{q}_1, \bar{\hat{q}}_1) = 12.92$ . The application of the  
 211 adaptive nudging decreases the distance between the time means to  $\mathcal{D}(\bar{q}_1, \bar{\tilde{q}}_1) = 2.65$ , thus shifting the whole  
 212 solution  $\tilde{q}_1$  much closer to the phase space region occupied by the reference solution. It also yields a lot  
 213 more accurate mean distance  $\langle \mathcal{D}(\tilde{q}_1, \bar{\tilde{q}}_1) \rangle = 12.6$ , thus suggesting that the solution has correct amplitude.  
 214 On the other hand,  $\langle \mathcal{D}(q_1, \bar{\tilde{q}}_1) \rangle = 12.2$  (which is quite close to  $\langle \mathcal{D}(\tilde{q}_1, \bar{\tilde{q}}_1) \rangle = 12.6$ ) thus reassuring once again  
 215 that the reconstructed model gives an adequate approximation of the reference flow dynamics. Note that  
 216 the perfect reconstruction over a period  $[0, T]$  would mean that  $\mathcal{D}(q_1(t), \tilde{q}_1(t)) = 0, t \in [0, T]$ .

## 217 4. Conclusions and discussion

218 In this study we proposed a method for preserving nominally-resolved flow patterns in low-resolution  
 219 ocean model simulations. The method utilizes the well-known idea of reconstructing the dynamical system  
 220 that underlies the observed flow evolution. However, direct application of this idea to the quasi-geostrophic  
 221 model studied in this work is numerically unfeasible task because of the high dimensionality of the observed  
 222 flow. Moreover, a numerical integration of the reconstructed dynamical system can be unstable, but our  
 223 methodology can cope with this and ensure stability. We solved the problem of large dimensionality by  
 224 applying the Empirical Orthogonal Function decomposition of the reference solution (the high-resolution  
 225 solution subsampled on the coarse grid) that allowed to reduce the dimension by three orders of magnitude.  
 226 In order to solve the unstable integration problem, we developed the adaptive nudging method following

227 (Shevchenko and Berloff, 2021). This method keeps the solution in the neighbourhood of the phase space  
 228 region occupied by the reference solution. This is sufficient for accurate reproduction of both the large-  
 229 and small-scale flow features at low resolutions, despite the fact that these features are not present in the  
 230 dynamical solutions of the low-resolution model. The proposed method aims to operate with hundreds of  
 231 degrees of freedom thus offering orders-of-magnitude acceleration compared to low-resolution ocean models  
 232 which have at least 3-4 orders of magnitude more.

233 The proposed method can formally be classified as a reduced order modelling method (e.g., Brunton  
 234 et al. (2016)), since it reduces the dimensionality of the original system. The principal difference of the  
 235 proposed method (compared to the reduced order modelling technique) is that it does not use the original  
 236 equation to substitute the reference solution projected onto the EOF basis functions. Instead, it reconstructs  
 237 a dynamical system describing PCs directly and then finds the solution by using leading EOF-PC pairs.  
 238 The dynamical system reconstruction used in this study is not a new idea, while using the adaptive nudging  
 239 method is a novel approach in itself not to mention its application in the context of dynamical systems  
 240 reconstruction. Moreover, a combination of the polynomial basis with the Fourier series is another new idea  
 241 which can find its use beyond the scope of this work.

242 The proposed method was tested on a 3-layer quasi-geostrophic ocean circulation model at low non-  
 243 eddy-resolving resolution, such that it cannot simulate the correct large-scale flow structure. Our results  
 244 show that if the reconstructed dynamical model is based only on the second-order polynomials, then it is not  
 245 sufficiently accurate (compared with the reference solution), because its time-mean eastward jet separation  
 246 point is shifted north, and the jet itself has unrealistic fluctuations which are not observed in the reference  
 247 solution. We tried to use higher order polynomials, but the reconstructed system became very sensitive  
 248 to errors leading to severe numerical instabilities which we failed to stabilize. We resolved this problem by  
 249 augmenting the polynomial basis with the additional Fourier series. With all this in place, not only the  
 250 large-scale flow structure becomes correct but also the small-scale coherent vortices, which are unresolved  
 251 in the low-resolution full-dynamics model, appear in the solution. All in all, this shows that the method has  
 252 potential for modelling even more complicated oceanic flows. Being small-scales-unaware (not relying on  
 253 reproducing the effect of small scales onto large ones like parameterisations), the proposed method can be  
 254 thought of as an alternative to the modern (small-scales-aware) parameterisations, which try to reproduce  
 255 effects of small dynamically unresolved scales on the large scales, in the hope that the solution will stay in the  
 256 right region of the phase space. The proposed approach is quite the opposite: it forces the solution to stay in  
 257 the right phase space region and predicts the flow evolution via the reconstructed reduced dynamical system.  
 258 Note that the method does not require the original quasi-geostrophic model to be solved at low-resolution.

259 It is worth reiterating again that the proposed method maintains the large-scale flow structure (the  
 260 eastward jet extension of the western boundary currents) and small-scale features (nominally resolved on  
 261 the coarse grid eddies) akin to those of the reference solution. Moreover, not only the nominally-resolved flow  
 262 structures are present in the modelled solution but also realistic vortex trajectories are correctly reproduced.  
 263 However, it does not mean that the exact same individual eddies in the sub-sampled high resolution solution  
 264 are preserved.

265 One of the important and general conclusions that can be drawn from our results is that not only  
 266 mesoscale eddy parameterization is possible in principle but also it can be highly accurate (up to reproducing  
 267 individual vortices) for significantly reduced dynamics (down to 30 degrees of freedom). This conclusion  
 268 provides great optimism for the ongoing parameterization studies, which are still far away from being  
 269 completed.

270 The reference data is used twice: first, for reconstructing the dynamical system; second, for augmenting  
 271 the solution of this system by nudging (to compute the PCs,  $\mathbf{y}(\mathbf{t})$ , in the nudging term in equation (7)).  
 272 The method can be further improved by using a more sophisticated nudging methodologies and different  
 273 dynamical systems which can better represent the underlying flow dynamics. The proposed method can

274 be applied to primitive equations, but in this case reconstruction of the dynamical system will be more  
 275 subtle, as it will include more PCs and can require changes of the basis functions. Moreover, EOF analysis  
 276 might cease to work for time-dependent forcing and more sophisticated flow decompositions will therefore  
 277 be needed (see, e.g., Xie et al. (2018); Shady et al. (2021)). It is also important to note that the proposed  
 278 data-driven method requires the system to be statistically equilibrated, which is not the case in applications  
 279 that undergo regime transitions (e.g., forced climate projections or systems with multiple (statistically)  
 280 steady states). In other words, if the system has multiple attractors and only some of them are presented  
 281 in data then the proposed method can only reproduce the flow dynamics which is presented in data.

282 Another future extensions of this study can be exploring the possibility of generating a forcing for the  
 283 low-resolution ocean model, based on the EOFs and the adaptive nudging, perhaps with some ingredients  
 284 such as stochastic forcing.

## 285 5. Acknowledgments

286 The authors thank The Leverhulme Trust for the support of this work through the grant RPG-2019-024.  
 287 Pavel Berloff was supported by the NERC grants NE/R011567/1 and NE/T002220/1, and by the Moscow  
 288 Center of Fundamental and Applied Mathematics (supported by the Agreement 075-15-2019-1624 with the  
 289 Ministry of Education and Science of the Russian Federation).

## 290 References

- 291 Aguirre, L. and Letellier, C. (2009). Modeling nonlinear dynamics and chaos: A review. *Mathematical Problems in Engineering*,  
 292 2009:1–35.
- 293 Arakawa, A. (1966). Computational design for long-term numerical integration of the equations of fluid motion: two-dimensional  
 294 incompressible flow. Part I. *J. Comput. Phys.*, 1:119–143.
- 295 Berloff, P. (2015). Dynamically consistent parameterization of mesoscale eddies. Part I: simple model. *Ocean Model.*, 87:1–19.
- 296 Berloff, P. (2016). Dynamically consistent parameterization of mesoscale eddies. Part II: eddy fluxes and diffusivity from  
 297 transient impulses. *Fluids*, 1:1–19.
- 298 Berloff, P. (2018). Dynamically consistent parameterization of mesoscale eddies. Part III: Deterministic approach. *Ocean*  
 299 *Model.*, 127:1–15.
- 300 Brunton, S., Brunton, W., Proctor, J., Kaiser, E., and Kutz, N. (2017). Chaos as an intermittently forced linear system. *Nat.*  
 301 *Commun.*, 8:1–9.
- 302 Brunton, S., Proctor, J., and Kutz, N. (2016). Discovering governing equations from data by sparse identification of nonlinear  
 303 dynamical systems. *PNAS*, 113:3932–3937.
- 304 Cooper, F. and Zanna, L. (2015). Optimization of an idealised ocean model, stochastic parameterisation of sub-grid eddies.  
 305 *Ocean Model.*, 88:38–53.
- 306 Cotter, C., Crisan, D., Holm, D., Pan, W., and Shevchenko, I. (2019). Numerically modelling stochastic Lie transport in fluid  
 307 dynamics. *Multiscale Model. Simul.*, 17:192–232.
- 308 Cotter, C., Crisan, D., Holm, D., Pan, W., and Shevchenko, I. (2020a). A Particle Filter for Stochastic Advection by Lie  
 309 Transport (SALT): A case study for the damped and forced incompressible 2D Euler equation. *SIAM/ASA Journal on*  
 310 *Uncertainty Quantification*, 8:1446–1492.
- 311 Cotter, C., Crisan, D., Holm, D., Pan, W., and Shevchenko, I. (2020b). Data assimilation for a quasi-geostrophic model with  
 312 circulation-preserving stochastic transport noise. *Journal of Statistical Physics*, 179:1186–1221.
- 313 Cotter, C., Crisan, D., Holm, D., Pan, W., and Shevchenko, I. (2020c). Modelling uncertainty using stochastic transport noise  
 314 in a 2-layer quasi-geostrophic model. *Foundations of Data Science*, 2:173–205.
- 315 Danilov, S., Juricke, S., Kutsenko, A., and Oliver, M. (2019). Toward consistent subgrid momentum closures in ocean models.  
 316 In Eden, C. and A.Iske, editors, *Energy Transfers in Atmosphere and Ocean*, chapter 5, pages 145–192. Springer-Verlag.
- 317 Duan, J. and Nadiga, B. (2007). Stochastic parameterization for large eddy simulation of geophysical flows. *Proc. Am. Math.*  
 318 *Soc.*, 135:1187–1196.
- 319 Frederiksen, J., OKane, T., and Zidikheri, M. (2012). Stochastic subgrid parameterizations for atmospheric and oceanic flows.  
 320 *Phys. Scr.*, 85:068202.
- 321 Gent, P. and McWilliams, J. (1990). Isopycnal mixing in ocean circulation models. *J. Phys. Oceanogr.*, 20:150–155.
- 322 Grooms, I., Majda, A., and Smith, K. (2015). Stochastic superparameterization in a quasigeostrophic model of the Antarctic  
 323 Circumpolar Current. *Ocean Model.*, 85:1–15.

- 324 Haidvogel, D., McWilliams, J., and Gent, P. (1992). Boundary current separation in a quasigeostrophic, eddy-resolving ocean  
 325 circulation model. *J. Phys. Oceanogr.*, 22:882 – 902.
- 326 Hannachi, A., Jolliffe, I., and Stephenson, D. (2007). Empirical orthogonal functions and related techniques in atmospheric  
 327 science: A review. *Int. J. Climatol.*, 27:1119–1152.
- 328 Hundsdoerfer, W., Koren, B., van Loon, M., and Verwer, J. (1995). A positive finite-difference advection scheme. *J. Comput.*  
 329 *Phys.*, 117:35–46.
- 330 Jansen, M. and Held, I. (2014). Parameterizing subgrid-scale eddy effects using energetically consistent backscatter. *Ocean*  
 331 *Model.*, 80:36–48.
- 332 Juricke, S., Danilov, S., Koldunov, N., Oliver, M., Sein, D., Sidorenko, D., and Wang, Q. (2020a). A kinematic kinetic  
 333 energy backscatter parametrization: From implementation to global ocean simulations. *J. Adv. Model. Earth Syst.*,  
 334 12:2020MS002175.
- 335 Juricke, S., Danilov, S., Koldunov, N., Oliver, M., and Sidorenko, D. (2020b). Ocean kinetic energy backscatter parametrization  
 336 on unstructured grids: Impact on global eddypermitting simulations. *J. Adv. Model. Earth Syst.*, 12:2019MS001855.
- 337 Karabasov, S., Berloff, P., and Goloviznin, V. (2009). CABARET in the ocean gyres. *Ocean Model.*, 2–3:155–168.
- 338 Kondrashov, D. and Berloff, P. (2015). Stochastic modeling of decadal variability in ocean gyres. *Geophys. Res. Lett.*, 42:1543–  
 339 1553.
- 340 Kondrashov, D., Chekroun, M., and Berloff, P. (2018). Multiscale Stuart-Landau emulators: Application to wind-driven ocean  
 341 gyres. *Fluids*, 3:1–32.
- 342 Mana, P. P. and Zanna, L. (2014). Toward a stochastic parameterization of ocean mesoscale eddies. *Ocean Model.*, 79:1–20.
- 343 Mangiarotti, S. and Huc, M. (2019). Can the original equations of a dynamical system be retrieved from observational time  
 344 series? *Chaos*, 29:023133.
- 345 McWilliams, J. (1977). A note on a consistent quasigeostrophic model in a multiply connected domain. *Dynam. Atmos. Ocean*,  
 346 5:427–441.
- 347 Pedlosky, J. (1987). *Geophysical fluid dynamics*. Springer-Verlag, New York.
- 348 Preisendorfer, R. W. (1988). *Principal Component Analysis in Meteorology and Oceanography*. Elsevier, Amsterdam.
- 349 Ryzhov, E., Kondrashov, D., Agarwal, N., and Berloff, P. (2019). On data-driven augmentation of low-resolution ocean model  
 350 dynamics. *Ocean Model.*, 142:101464.
- 351 Ryzhov, E., Kondrashov, D., Agarwal, N., McWilliams, J., and Berloff, P. (2020). On data-driven induction of the low-frequency  
 352 variability in a coarse-resolution ocean model. *Ocean Model.*, 153:101664.
- 353 Sceller, L. L., Letellier, C., and G., G. (1999). Structure selection for global vector field reconstruction by using the identification  
 354 of fixed points. *Phys. Rev. E*, 60:1600–1606.
- 355 Shady, A., Suraj, P., Omer, S., Adil, R., and Mandar, T. (2021). A nudged hybrid analysis and modeling approach for realtime  
 356 wake-vortex transport and decay prediction. *Computers and Fluids*, 221:104895.
- 357 Shevchenko, I. and Berloff, P. (2015). Multi-layer quasi-geostrophic ocean dynamics in eddy-resolving regimes. *Ocean Modell.*,  
 358 94:1–14.
- 359 Shevchenko, I. and Berloff, P. (2016). Eddy backscatter and counter-rotating gyre anomalies of midlatitude ocean dynamics.  
 360 *Fluids*, 1(3):1–16.
- 361 Shevchenko, I. and Berloff, P. (2021). A method for preserving large-scale flow patterns in low-resolution ocean simulations.  
 362 *Ocean Model.*
- 363 Shevchenko, I., Berloff, P., Guerrero-Lóopez, D., and Roman, J. (2016). On low-frequency variability of the midlatitude ocean  
 364 gyres. *J. Fluid Mech.*, 795:423–442.
- 365 Shu, C. and Osher, S. (1988). Efficient implementation of essentially non-oscillatory shock-capturing schemes. *J. Comput.*  
 366 *Phys.*, 77:439–471.
- 367 Siegel, A., Weiss, J., Toomre, J., McWilliams, J., Berloff, P., and Yavneh, I. (2001). Eddies and vortices in ocean basin  
 368 dynamics. *Geophys. Res. Lett.*, 28:3183–3186.
- 369 Woodward, P. and Colella, P. (1984). The numerical simulation of two-dimensional fluid flow with strong shocks. *J. Comput.*  
 370 *Phys.*, 54:115–173.
- 371 Xie, X., Mohebujjaman, M., Rebholz, L., and Iliescu, T. (2018). Data-driven filtered reduced order modeling of fluid flows.  
 372 *SIAM J. Sci. Comput.*, 40:B834–B857.